

LIR: A Lightweight Baseline for Image Restoration

Dongqi Fan, Ting Yue, Xin Zhao, and Liang Chang

University of Electronic Science and Technology of China, Chengdu, CN
{dongqifan, yueting, xinzhao}@std.uestc.edu.cn
liangchang@uestc.edu.cn

Abstract. Recently, there have been significant advancements in Image Restoration based on CNN and transformer. However, the inherent characteristics of the Image Restoration task are often overlooked. Many works, instead, only focus on the basic block design and stack numerous such blocks to the model, leading to parameters redundant and computations unnecessary. Thus, the efficiency of the image restoration is hindered. In this paper, we propose a Lightweight Baseline for Image Restoration called LIR to efficiently reconstruct the image and remove degradations (blur, rain, noise, haze). First of all, LIR addresses the degradations existing in the local and global residual connections that are ignored by modern networks, through a simple structural design. Then, to achieve lightweight, a Lightweight Adaptive Attention (LAA) Block is introduced depending on the inherent characteristics of the Image Restoration, which is mainly composed of proposed Adaptive Filters and Attention Blocks. LAA is capable of adaptively sharpening contours, removing degradation, and capturing global information in various Image Restoration scenes in a computation-friendly manner. Extensive experiments demonstrate that our LIR achieves comparable performance to state-of-the-art models with fewer parameters and computations in certain tasks. In addition, it is worth noting that our LIR produces better visual results than state-of-the-art networks that are more in line with the human aesthetic. The code is available at: <https://github.com/Dongqi-Fan/LIR>

Keywords: Image Restoration · Lightweight · Attention

1 Introduction

Image Restoration (IR) is a fundamental computer vision task aiming to reconstruct a degraded image into a clean one, including deblurring, deraining, etc. In recent years, we have witnessed the great process of deep learning methods [28, 33, 39, 52, 54, 59, 67] in IR. However, many existing works only focus on designing the basic block and inefficiently stacking these blocks in a model, without considering the specific characteristics of the IR task. This approach often

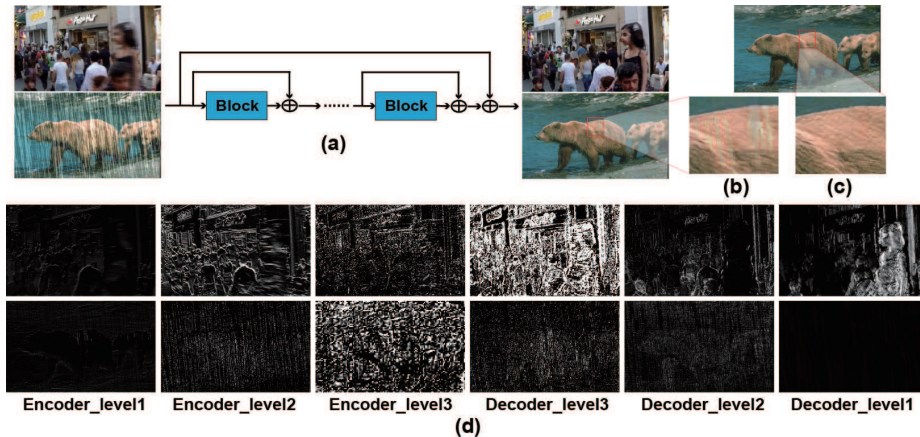


Fig. 1: Visualization experiment of the image restoration process. (a) The paradigm of the most modern networks that incorporate both local and global residual connections. (b) The output by Restormer still exhibits visible traces of rain. (c) The output of our LIR. Which is more plain and solves the problem of residual connections carrying degradation. (d) The visualization of the three levels of the encoder and decoder based on Restormer. The top is deblurring and bottom is deraining.

leads to parameter redundancy and computations unnecessary. Instead, our goal is an efficient and lightweight network design for various IR tasks.

To address the issue of vanishing gradient and stabilize training, as shown in Fig. 1 (a), most modern networks usually incorporate local and global residual connections. However, we think that these connections may propagate the degradation of the input throughout the entire network and introduce it into the reconstructed clean output. To validate our idea, we conduct visualization experiments on the deblurring and deraining tasks using Restormer [58], a transformer model with a U-Net structure. Fig. 1 illustrates the feature maps output by the encoder and decoder at three levels, as well as the input and output images of the Restormer, on the deblurring (at the top of Fig. 1 (d)) and deraining (at the bottom of Fig. 1 (d)) task. Notably, at the bottom of Fig. 1 (d), it is evident that each feature map and the final output of the network (Fig. 1 (b)) all contain degradation (rain). Although less pronounced in the deblurring task, a similar phenomenon can be observed at the top of Fig. 1 (d). To overcome this issue, we use an ingenious structural design (transpose branches in the LIR and LAA Fig. 2) that effectively eliminates the degradation in the local and global residual connections. Fig. 1 (c) shows the restored image output by our LIR, which is more plain than the Restormer (Fig. 1 (b)).

Moreover, we observe another serious issue in the visualization. In the visualization of the deblurring task (at the top of Fig. 1 (d)), the feature maps generated by encoder_level2 and decoder_level2 exhibit clear contours while the other feature maps exhibit blurred contours. This issue is even worse in the deraining (at the bottom of Fig. 1 (d)) task. All feature maps not only display

very blurry contours but also contain a considerable amount of noise. Especially for the feature map generated by `decoder_level1`, it shows barely discernible contours, only with faint traces of rain. The more important is that the high-frequency information has been lost. These observations indicate that although many modern networks have achieved satisfactory results on the metric (PSNR), the restoration process of the image is highly inefficient and fails to address the core issues of image restoration, thus resulting in poor visual quality. Based on this insight, we propose the Adaptive Filter (Fig. 3) (an component of the LAA) as a solution to adaptively extract high-frequency information, enhance object contours, and remove degradation in various IR tasks.

Transformer-based models have demonstrated impressive performance in various tasks, both at high-level [9, 12, 31, 49] and low-level [3, 6, 27, 51, 54]. However, there exist different opinions. [10] argues that attention is not all you need, emphasizing the importance of skip connections and Multi-layer Perceptrons (MLPs). In addition, [29, 47, 48] share a similar viewpoint that highlights the potential of MLPs beyond transformers. On the other hand, [50] suggests that CNN can achieve comparable results to transformers by leveraging the attention mechanism and patch embedding strategy. Thus, excessive computations can be avoided. Furthermore, [8, 16, 32, 70] take advantage of the attention mechanism in the CNN along with large convolution kernels to capture global information, instead of the self-attention among the transformer. Satisfactory results are achieved and excessive computations are avoided. Inspired by these perspectives, through leveraging the patch embedding strategy and MLP, we propose the Patch Attention module (Fig. 4) (an component of the Attention Block) that aims to capture global information of the features and keeps parameters and computations friendly.

In this paper, we propose a Lightweight Image Restoration network called LIR (Fig. 2) to efficiently remove degradation and adapt to various IR tasks. The key component of LIR is the novel Lightweight Adaptive Attention Block (LAA) consisting of several proposed Adaptive Filters and Attention Blocks. Furthermore, the Attention Block is formed by proposed Patch Attention module (Fig. 4), ResCABlock, and ResBlock (Details can be found in Fig. 2). Thanks to the Adaptive Filter and Attention Block, the LAA Block is not only able to adaptively enhance the object contour and remove degradation but also to capture global information. Furthermore, we address the issue of degradation existing in the local and global residual connections by subtracting the output of the later component from the output of the first component in the LIR and LAA Block. This subtraction allows us to obtain the degradation, which is then expanded through the Transpose operation. After that, we subtract this expanded degradation from the residual connection to obtain a clean residual connection. Extensive experiments demonstrate that LIR achieves comparable performance to state-of-the-art models in PSNR and produces better visual results that are more in line with the human aesthetic.

Our contributions can be summarized as follows:

- Through a simple structural design, the problem that local and global residual connections bring degradation is addressed, which is overlooked by modern networks.
- Given the problem of the loss of high-frequency information observed in the visualization experiments, we propose the Adaptive Filter (Fig. 3) as a solution to adaptively extract high-frequency information and enhance object contours.
- To give LIR the ability to extract global information, we propose the Patch Attention module (Fig. 4), which is more computation-friendly than the self-attention of the transformer.
- Based on Adaptive Filter, Patch Attention, ResCABlock, and ResBlock, we designed a lightweight and powerful block: LAA. It can make the LIR achieve comparable performance to state-of-the-art networks and better visual effects with smaller parameters and computations.

2 Related Work

2.1 Image Restoration

In recent years, IR based on deep learning methods [13, 19, 26, 55, 61, 63] have shown promising results. The transformer architectures achieve adaptive spatial aggregation at the cost of heavy computation. To address this challenge, a Kernel Basis Attention (KBA) module has been proposed by KNet [67] in the CNN. It adaptively aggregates spatial neighborhood information in a kernel-wise manner, thereby reducing computation. ADMS [38] proposes a Filter Attribution method based on Integral Gradient (FAIG) [55] to identify the contributions of the filters to remove specific degradations. By masking filters with minimal impact on degradation removal, the network’s efficiency in removing degradations is improved. IDR [61] proposes a learnable Principal Component Analysis (PCA) and views various IR tasks as multi-task learning methods to obtain network priors and remove degradations. MPRNet [59] introduces the Multi-Stage Progressive Restoration method, which is based on the U-Net architecture and follows a multi-input multi-output style. In addition, the contrastive learning paradigm is utilized by AirNet [24] to train the network to deal with different unknown degradations. Through the prompting of the contrastive learning paradigm, the latent features in the network gradually away from the degradation space and close to the clean space. Different from the above works, our emphasis is on lightweight and efficient design while ensuring good performance.

2.2 Vision Transformer for Image Restoration

IPT [3] is the first work that introduces ViT [12] to low-level tasks to achieve image super-resolution, denoising, and deraining. The computational complexity of the self-attention part in ViT is $O(N^2D)$, where $N = H \times W$ represents the length of the patch sequence and D represents the dimension of the sequence.

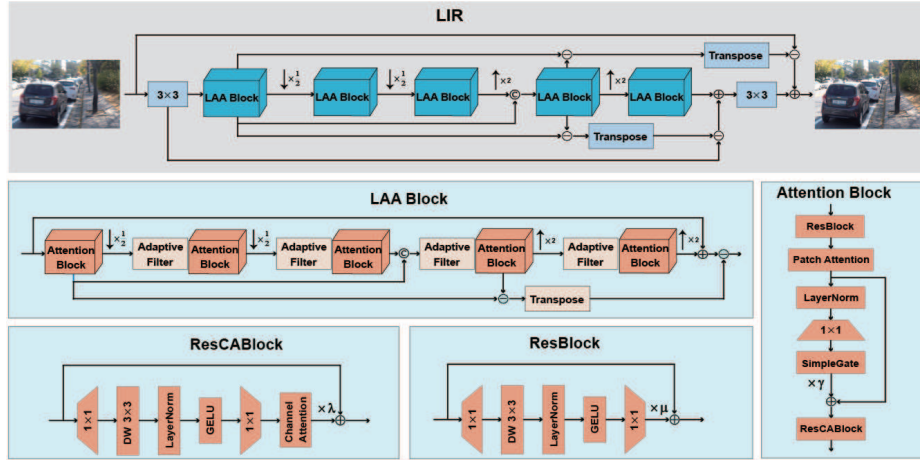


Fig. 2: The detailed structure of the proposed Lightweight Image Restoration (LIR) network, which is mainly stacked by Lightweight Adaptive Attention (LAA) Blocks. Thanks to the Adaptive Filter, Patch Attention, ResCABlock, and the ResBlock, the LAA Block is endowed with the ability to extract a variety of information efficiently.

Although vision transformers are capable of capturing long-range dependencies, the self-attention component imposes a significant computing burden. The computational complexity of the self-attention increases quadratically with the input size. To mitigate this issue, TransWeather [53] introduces a reduction ratio factor R to control the complexity, resulting in a computational complexity of $O(N^2D/R)$. Uformer [54] and StripFormer [51] proposes the window and stripe attention mechanisms respectively, which reduce the computational complexity to $O(NM^2D)$ and $O(D(H^2W + HW^2))$ by calculating dependencies in smaller windows and strips, where M represents the window size. To further reduce the computational complexity, [22] estimates the attention map that is output by the self-attention part using an element-wise product operation in the frequency domain, and GRL [27] proposes an anchor stripe attention mechanism to further narrow down the computational range of the self-attention. The computational complexities are reduced to $O(N \log ND)$ and $O(NMD)$ respectively, where M represents the size of feature map. However, the computation required for self-attention remains unaffordable. To address this issue, we propose a novel Patch Attention module to approximate the self-attention part by simplifying two matrix multiplications into one element-wise multiplication and removing the softmax operation, leading to significant computational savings.

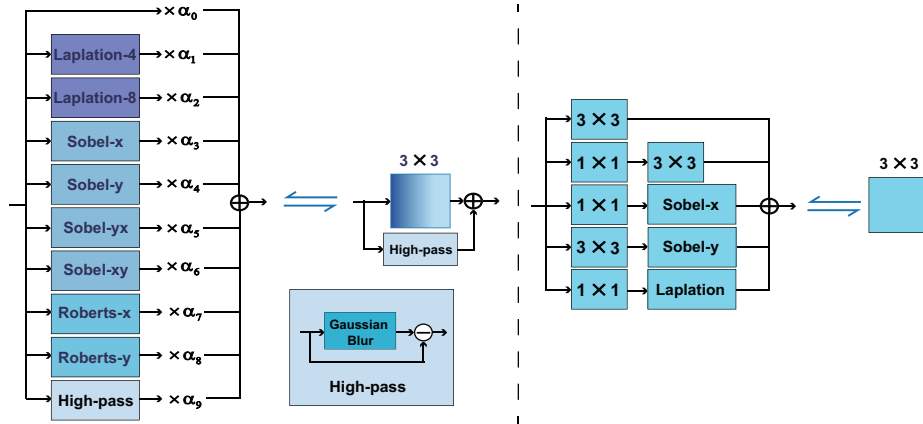


Fig. 3: The comparison between our Adaptive Filter (left) and Edge-oriented Convolution Block (right). Both are reparameterization style that multiple convolutions are reparameterized into one during inference after the training.

3 Method

3.1 Lightweight Image Restoration

The overall structure of LIR is illustrated in Fig. 2, which primarily consists of Lightweight Adaptive Attention (LAA) Blocks. Both LIR and LAA Block adopt a down-up style to reduce computation and save parameters, that is downsizing the feature map in the beginning and upsizing at the end. To preserve low-frequency information and ensure training is stable, we add two global residual connections into LIR. One connects the input of the network to the output, while the other connects the head 3×3 Conv to the tail 3×3 Conv.

As mentioned in Sec. 1, these residual connections can bring degradation. To address this, we subtract the output of the fourth LAA Block from the output of the first LAA Block to obtain the corresponding degradation. We then amplify the degradation through the Transpose operation and subtract it from the residual connection to obtain a clean connection. The same approach is used to remove degradation in the local residual connection within the LAA Block, where we subtract the output of the fourth Attention Block from the output of the first Attention Block to obtain the corresponding degradation. The reason we adopt this method is that the feature map of the shallow layer contains more degradation compared to a deep layer. Thus, this design allows the network to dynamically perceive this difference between shallow and deep layers during the training process and inference stage. Now, the problem that local and global residual connections bring degradation is addressed. Next, we illustrate how we can achieve lightweight and efficiency through the Adaptive Filter and Attention Block in detail.

3.2 Adaptive Filter

To achieve lightweight and efficiency, we first introduce the Adaptive Filter (at the left of Fig. 3), inspired by Edge-oriented Convolution Block (ECB) [66] (at the right of Fig. 3). The rich filters of different kinds allow the AF to enhance the object contour, remove degradation, and extract useful high-frequency information. Furthermore, the LAA block can be reparameterized as one 3×3 and one high-pass filter after training to achieve lightweight.

Although Adaptive Filter shares similarities with the ECB, it significantly outperforms ECB in three ways. Firstly, the ECB introduces more convolution operations during training leading to more training costs (i.e. parameters and computations). Instead, our Adaptive Filter only requires 10 training parameters resulting in smaller training costs. Secondly, the Adaptive Filter can be applied to various IR scenes and dynamically adjust the dependence on different filters by adjusting parameters α . However, the ECB treats each branch equally and can not adapt to various IR scenes. Lastly, the Adaptive Filter offers a wider range of filters that can extract more types of useful information and is more robust to noisy scenes, while the ECB is brittle in rich degradation scenes.

Each filter in the Adaptive Filter has its own advantages and disadvantages. Thus, we use the learnable parameters α to adaptively maximize their advantages and minimize their disadvantages in different LAA blocks of the LIR. Specifically, in these filters, the **Roberts filter** is used to detect the pixel changes in the features by the differential method. It is effective in extracting prominent edges but fails to detect details. Where Roberts-x and Roberts-y represent the detection in the horizontal direction and vertical direction; The **Sobel filter** extracts edge information by approximating first-order differentials discretely. It has some resistance to noise and a good ability to detect details. However, the Sobel filter may cause edge thinning and false detection in scenes with a mass of noise; The **Laplacian filter** extracts edge information by approximating second-order differentials discretely. It can detect more detailed edges and textures than Sobel but is more sensitive to noise and may result in a bilateral effect on the edges. Where Laplacian-4 and Laplacian-8 represent 4 domains and 8 domains; The **high-pass filter** obtains high-frequency information by subtracting the features after Gaussian blur processing from the original features. This filter is more robust in noisy scenes compared to the above filters; Finally, we add a **residual connection** to the AF for stages where the features have scarce noise and a clear outline.

3.3 Attention Block

While different types of filters in Adaptive Filter (AF) enable LAA blocks to extract rich information, AF alone is not enough, as we need to take full advantage of the rich information extracted by AF. Thus, a strong and efficient Attention Block is introduced, which consists of four components: ResBlock, Patch Attention (PA), SimpleGate, and ResCABlock. We first use the ResBlock to preprocess input features, followed by the extraction of global information

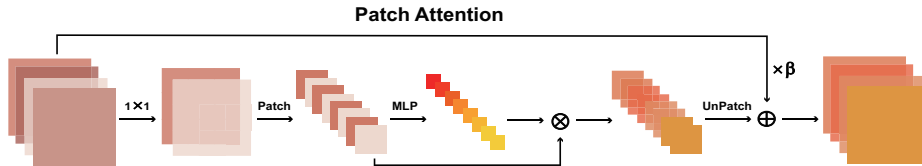


Fig. 4: The flow of the proposed Patch Attention.

using our PA module. The efficacy of the gate function has been demonstrated in prior research [4, 29, 52]. Here, we simply employ the SimpleGate module from [4] to further extract dependencies between features. Finally, we leverage the ResCABlock to extract channel-wise information.

ResBlock and ResCABlock Both ResBlock and ResCABlock are up-down style residual blocks that include a learnable parameter in the trunk. The only difference between ResBlock and ResCABlock is that the latter has a channel attention module at the tail. The Channel Attention module [68], based on Squeeze-and-Excitation (SE) [17], has gained much popularity for its ability to extract channel-wise information. Many studies [4, 6, 27, 69] have directly utilized this module in their models. Following them, in our Attention Block, we also incorporate the Channel Attention module into the ResBlock to extract channel-wise information. In addition, the structure of ResBlock and ResCABlock are designed to be simple to meet lightweight and efficient requirements.

Patch Attention To give the Attention Block the ability to capture global information, we introduce the Patch Attention (PA) (Fig. 4). In the self-attention part of the transformer, the attention map is calculated using two matrix multiplications and a softmax operation between q , k , and v , which incurs significant computational overhead. Instead, we simplify the attention map computation in our PA by using just one MLP and one element-wise multiplication.

Specifically, we set C , H , and W as the channel, height, and width of the feature map, and (P_h, P_w) as patch size. The C_{scale} is used to control the dimension of the channel. We start by reducing the dimension of the input feature map from (C, H, W) to $(C/C_{scale}, H, W)$ using a 1×1 convolution. Next, we divide the feature map into non-overlapping patches and reshape it into $(HW//P_hP_w, P_hP_wC//C_{scale})$. Then, we feed this reshaped feature into the MLP to obtain the attention weights for each patch $(HW//P_hP_w, 1, 1)$. Finally, we perform element-wise multiplication between the obtained attention weights and the input feature map to capture global information. It is important to note that our attention weights have a smaller dimension, resulting in a lower computation scale to self-attention. The (P_h, P_w) in the LIR is set to $(8, 8)$, $(4, 4)$, and $(2, 2)$ respectively, and the C_{scale} is set to 16 and 8, according to the depth of the network.

Table 1: Image Deraining results evaluated by PSNR and SSIM on Rain100L dataset. Where \triangle stands for the official code that is unavailable or not based on PyTorch.

Method	Type	Rain100L [56]		Params [M]	GFLOPs
		PSNR \downarrow	SSIM		
UMRL [57]	CNN	29.18	0.923	0.98	9.31
PReNet [42]	RNN	32.44	0.950	0.17	37.27
AirNet [24]	CNN	34.90	0.966	8.93	169.47
MPRNet [59]	CNN	36.40	0.965	20.13	960.39
SPAIR [40]	CNN	36.93	0.969	\triangle	\triangle
HINet [5]	CNN	37.28	0.970	88.67	95.92
MAXIM-2S [52]	MLP	38.06	0.977	22.50	80.13
SFNet [7]	CNN	38.21	0.974	13.27	70.00
DRCNet [25]	CNN	38.23	0.976	18.90	\triangle
Restormer [58]	Transformer	38.99	0.978	26.13	79.31
LIR (Ours)	CNN	38.96	0.983	7.31	63.96

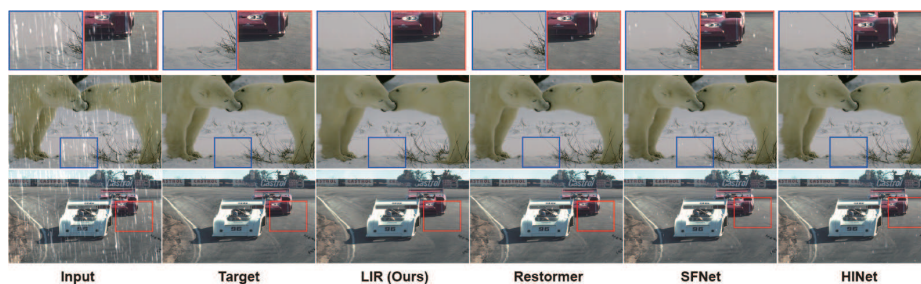


Fig. 5: The visual comparisons for LIR, Restormer [58], SFNet [7], and HINet [5]. LIR produces state-of-the-art visual results.

4 Experiment

4.1 Experiment Settings

We set the number of LAA Blocks in the LIR to [3,3,3,3,4], and the width to 48. During the training, we use the L_1 loss function, AdamW ($\beta_1=0.9$, $\beta_2=0.999$) optimizer with an initial learning rate of $3e^{-4}$, and set weight decay as $1e^{-4}$. Random image cropping and horizontal flipping are used as data augmentation strategies. Following [58], we use the cosine annealing strategy to gradually decrease the learning rate from $3e^{-4}$ to $1e^{-6}$, and use the progressive learning, where training patch size and batch size pairs are: [(128²,32), (160²,16), (256²,8)] at iterations [250K, 250K, 250K] for deblurring, deraining, and denoising. For dehazing, we set [(128²,32), (160²,16)] at iterations [350K, 400K]. The number of parameters and computation for each method are calculated based on the input size of (3,192,192). Specifically, parameters are counted using the PyTorch,

and the computation is measured using the thop package. All experiments are conducted using the official release code for each method. For methods that do not have released code or are not based on PyTorch, we have marked them with \triangle in the tables.

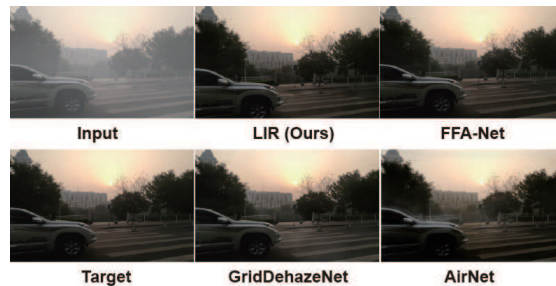


Fig. 6: The visual comparisons for LIR, FFA-Net [41], GridDehazeNet [30], and AirNet [24]. LIR produces better visual results.

4.2 Image Deraining

The Rain14000 [15] (11,200 training images) and Rain100H [56] (1,254 training images) are used to train LIR, and the Rain100L [56] datasets is used for evaluation. The results are presented in Tab. 1. In the Rain100L results (Tab. 1), LIR with minimal parameters and computation outperforms the DRCNet [25] and achieves comparable performance to Restormer [58] with only a slight 0.02 dB decrease on PSNR. In addition, our LIR achieves state-of-the-art on SSIM, which significantly outperforms Restormer. As GFLOPs do not accurately reflect the computations of the transformer model, the actual computation of LIR is much lower compared to Restormer, as shown in Tab. 1.

It is worth noting that with fewer parameters and computations, LIR significantly outperforms SFNet [7], the same lightweight design method as ours. Fig. 5 shows visual comparisons among LIR, Restormer, SFNet, and HINet. It can be demonstrated that LIR produces state-of-the-art visual results, despite LIR having a slightly lower PSNR than Restormer.

4.3 Image Dehazing

The OTS [23] (72,315 training images) is used to train LIR, and the Synthetic Objective Testing Set (SOTS) outdoor [23] is used for evaluation. In the SOTS outdoor results (Tab. 2), LIR significantly outperforms both the MAXIM-2S [52] (MLP-based) and the U2-Former [20] (transformer-based) with improvement in PSNR of 0.66 dB and 3.75 dB. In addition, LIR achieves comparable performance on PSNR and better performance on SSIM to DehazeFormer. It is worth noting

Table 2: Image dehazing results evaluated by PSNR and SSIM on SOTS outdoor dataset. Where \triangle stands for the official code that is unavailable or not based on PyTorch.

Method	Type	SOTS outdoor [23]		Params [M]	GFLOPs
		PSNR \downarrow	SSIM		
FD-GAN [11]	GAN	23.15	0.920	13.98	38.90
AirNet [24]	CNN	23.18	0.900	8.93	169.47
IDR [62]	CNN	25.24	0.943	15.34	\triangle
GridDehazeNet [30]	CNN	30.86	0.982	0.96	12.05
U2-Former [20]	Transformer	31.10	0.976	\triangle	\triangle
FFA-Net [41]	CNN	33.38	0.980	4.46	161.74
MAXIM-2S [52]	MLP	34.19	0.985	22.5	80.13
DehazeFormer [44]	Transformer	34.95	0.984	2.52	13.37
LIR (Ours)	CNN	34.85	0.985	7.31	63.96

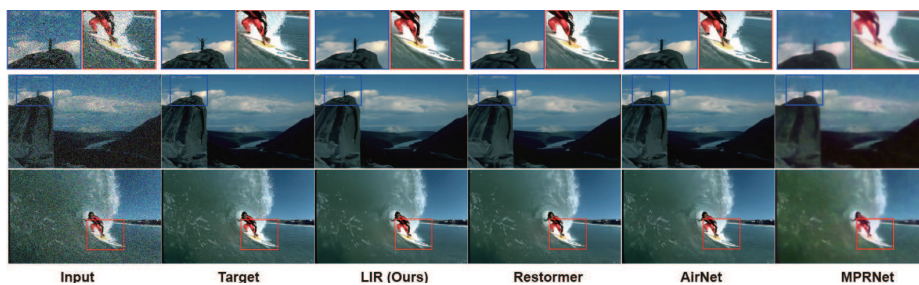


Fig. 7: The visual comparisons for LIR, Restormer [58], AirNet [24], and MPRNet [59]. LIR produces state-of-the-art visual results.

that GFLOPs and parameters do not accurately reflect the complexity of the transformer model, the actual complexity of LIR is much lower compared to DehazeFormer. Visual comparisons are shown in the Fig. 6.

4.4 Image Denoising

We perform denoising experiments on synthetic benchmark datasets generated by additive white Gaussian noise. The DFWB (DIV2K [1], Flickr2K, WED [34], BSD500 [2]) datasets with 8,594 training images are used to train LIR. For evaluation, we use the CBSD68 [35] and Urban100 [18] datasets. The light blue color in the Tab. 3 indicates that the method is trained using a blind denoising setting (random σ from [0,50]) and then evaluated under a fixed σ (0, 25, or 50). Other methods are trained with a fixed σ and evaluated with the same σ as training. As shown in the Tab. 3, LIR achieves comparable performance to Restormer [58] and significantly outperforms all other models on the CBSD68 dataset with a blind denoising setting. Moreover, it is worth noting that with a 77% reduction in parameters and a 20% reduction in computations, our LIR achieves comparable

Table 3: Image denoising results evaluated by PSNR and SSIM on CBS68 and Urban100 datasets. Where \triangle stands for the official code that is unavailable or not based on PyTorch and light blue for the method that is learned to handle various noise levels.

Method	Type	CBS68 [35] \downarrow			Urban100 [18]			Params [M]	GFLOPs
		$\sigma = 15$	$\sigma = 25$	$\sigma = 50$	$\sigma = 15$	$\sigma = 25$	$\sigma = 50$		
FD-GAN [11]	GAN	30.25	28.81	26.43	-	-	-	13.98	38.90
DL [14]	CNN	33.05	30.41	26.90	-	-	-	\triangle	\triangle
MPRNet [59]	CNN	33.54	30.89	27.56	-	-	-	20.13	960.39
AirNet [24]	CNN	33.92	31.26	28.00	34.40	32.10	28.88	8.93	169.47
BRDNet [46]	CNN	34.10	31.43	28.16	34.42	31.99	28.56	\triangle	\triangle
IDR [62]	CNN	34.11	31.60	28.14	33.82	31.29	28.07	15.34	\triangle
DRUNet [64]	CNN	34.30	31.69	28.51	34.81	32.60	29.61	32.64	80.78
Restormer [4]	Transformer	34.39	31.78	28.59	35.06	32.91	30.02	26.13	79.31
LIR (Ours)	CNN	34.31	31.69	28.50	34.81	32.59	29.57	7.31	63.96

Table 4: Image deblurring results evaluated by PSNR and SSIM on GoPro and HIDE datasets. Where \triangle stands for the official code that is unavailable or not based on PyTorch.

Method	Type	GoPro [36]		HIDE [43]		Params [M]	GFLOPs
		PSNR \downarrow	SSIM	PSNR \downarrow	SSIM		
IDR [62]	CNN	27.87	0.846	-	-	15.34	\triangle
DBGAN [65]	GAN	31.10	0.942	28.94	0.915	11.58	189.71
MT-RNN [37]	RNN	31.15	0.945	29.15	0.918	\triangle	\triangle
DMPHN [60]	CNN	31.20	0.940	29.09	0.924	21.70	\triangle
Zhe et al. [21]	CNN	31.79	0.949	-	-	\triangle	\triangle
Suin et al. [45]	CNN	31.85	0.948	29.98	0.939	\triangle	\triangle
SPAIR [40]	CNN	32.06	0.950	30.29	0.931	\triangle	\triangle
LIR (Ours)	CNN	32.19	0.931	30.31	0.917	7.31	63.96

performance to DRUNet [64] on Urban100, while the DRUNet is trained under fixed σ setting and our LIR is under random σ setting. The visual comparisons between LIR, Restormer, AirNet, and MPRNet are shown in Fig. 7. Although LIR is not as high as Restormer on PSNR, the state-of-the-art visual result is achieved.

4.5 Image Deblurring

The GoPro [36] (2,103 training images) dataset is used to train LIR, and the GoPro (1,111 images) and HIDE [43] (2,025 images) datasets are used for evaluation. Tab. 4 demonstrates that our LIR significantly outperforms other methods with fewer parameters and computations. Specifically, LIR is 0.13 dB higher than SPAIR [40], and 0.34 dB significantly higher than Suin et al [45].

Table 5: Ablation studies are performed on Rain100L dataset.

Metric	Baseline	Simple Residual	Patch Attention	Adaptive Filter
PSNR	38.96	38.87	38.85	38.66
Params [M]	7.31	6.86	6.51	7.31
GFLOPs	63.96	49.15	62.15	62.40

4.6 Ablation Studies

We conduct ablation experiments on the Rain100L dataset, using unchanged LIR as the baseline. The ablation experiments are performed on three types: Simple Residual, No Patch Attention, and No Adaptive Filter. Simple Residual refers to using vanilla global and local residual connections in the model, without removing the degradation in residual connections through structural design. In addition, No Adaptive Filter refers to using a vanilla convolution to replace the Adaptive Filter for fair comparison. Therefore, the number of parameters is unchanged. The results in the Tab. 5 demonstrate that the absence of the Adaptive Filter has the greatest negative impact on LIR. In addition, the experiment without Patch Attention demonstrates that our proposed Patch Attention module is efficient and computation-friendly, only bringing 0.8 M parameters and 1.81 GFLOPs computations.

5 Conclusion and Limitation

5.1 Conclusion

In this paper, we introduce a Lightweight Image Restoration network called LIR, which aims to efficiently remove degradation. Firstly, the problem that local and global residual connections propagate the degradation throughout the entire network is addressed through the use of the Transpose operation and a simple structural design. In addition, we propose the Adaptive Filter (AF) to adaptively extract high-frequency information, enhance object contours, and eliminate degradation in various IR tasks. Our AF achieves promising results while requiring minimal parameters and computations, as demonstrated in our ablation studies (Tab. 5). To capture global information while keeping small parameters and low computational requirements, we introduce the Patch Attention (PA) module by leveraging an MLP and patch embedding strategy.

5.2 Limitation

For the deraining task, LIR achieves comparable performance with the state-of-the-art method on PSNR and the best performance on SSIM with smaller parameter numbers and computations; For denoising and dehazing tasks, LIR also achieves comparable performance to the state-of-art method. In addition,

LIR achieves state-of-the-art visual results on deraining and denoising tasks. However, as Tab. 4 shows, LIR is less prominent on deblurring tasks than deraining and denoising. We believe that this is because, in the deblurring task, object outlines tend to be stretched out very long. While our Adaptive Filter is very effective when dealing with static object contours, it has limitations when dealing with dynamic contours caused by fast-moving objects.

References

1. Agustsson, E., Timofte, R.: Ntire 2017 challenge on single image super-resolution: Dataset and study. In: Proceedings of the IEEE conference on computer vision and pattern recognition workshops. pp. 126–135 (2017)
2. Arbelaez, P., Maire, M., Fowlkes, C., Malik, J.: Contour detection and hierarchical image segmentation. *IEEE transactions on pattern analysis and machine intelligence* **33**(5), 898–916 (2010)
3. Chen, H., Wang, Y., Guo, T., Xu, C., Deng, Y., Liu, Z., Ma, S., Xu, C., Xu, C., Gao, W.: Pre-trained image processing transformer. In: Proceedings of the IEEE/CVF conference on computer vision and pattern recognition. pp. 12299–12310 (2021)
4. Chen, L., Chu, X., Zhang, X., Sun, J.: Simple baselines for image restoration. In: European Conference on Computer Vision. pp. 17–33. Springer (2022)
5. Chen, L., Lu, X., Zhang, J., Chu, X., Chen, C.: Hinet: Half instance normalization network for image restoration. In: Proceedings of the IEEE/CVF Conference on Computer Vision and Pattern Recognition. pp. 182–192 (2021)
6. Chen, X., Wang, X., Zhou, J., Dong, C.: Activating more pixels in image super-resolution transformer. arXiv 2022. arXiv preprint arXiv:2205.04437 **1** (2022)
7. Cui, Y., Tao, Y., Bing, Z., Ren, W., Gao, X., Cao, X., Huang, K., Knoll, A.: Selective frequency network for image restoration. In: The Eleventh International Conference on Learning Representations (2022)
8. Ding, X., Zhang, X., Han, J., Ding, G.: Scaling up your kernels to 31x31: Revisiting large kernel design in cnns. In: Proceedings of the IEEE/CVF conference on computer vision and pattern recognition. pp. 11963–11975 (2022)
9. Dong, X., Bao, J., Chen, D., Zhang, W., Yu, N., Yuan, L., Chen, D., Guo, B.: Cswin transformer: A general vision transformer backbone with cross-shaped windows. In: Proceedings of the IEEE/CVF Conference on Computer Vision and Pattern Recognition. pp. 12124–12134 (2022)
10. Dong, Y., Cordonnier, J.B., Loukas, A.: Attention is not all you need: Pure attention loses rank doubly exponentially with depth. In: International Conference on Machine Learning. pp. 2793–2803. PMLR (2021)
11. Dong, Y., Liu, Y., Zhang, H., Chen, S., Qiao, Y.: Fd-gan: Generative adversarial networks with fusion-discriminator for single image dehazing. In: Proceedings of the AAAI Conference on Artificial Intelligence. vol. 34, pp. 10729–10736 (2020)
12. Dosovitskiy, A., Beyer, L., Kolesnikov, A., Weissenborn, D., Zhai, X., Unterthiner, T., Dehghani, M., Minderer, M., Heigold, G., Gelly, S., et al.: An image is worth 16x16 words: Transformers for image recognition at scale. arXiv preprint arXiv:2010.11929 (2020)
13. Du, W., Chen, H., Yang, H.: Learning invariant representation for unsupervised image restoration. In: Proceedings of the IEEE/CVF conference on computer vision and pattern recognition. pp. 14483–14492 (2020)

14. Fan, Q., Chen, D., Yuan, L., Hua, G., Yu, N., Chen, B.: A general decoupled learning framework for parameterized image operators. *IEEE transactions on pattern analysis and machine intelligence* **43**(1), 33–47 (2019)
15. Fu, X., Huang, J., Zeng, D., Huang, Y., Ding, X., Paisley, J.: Removing rain from single images via a deep detail network. In: *Proceedings of the IEEE conference on computer vision and pattern recognition*. pp. 3855–3863 (2017)
16. Guo, M.H., Lu, C.Z., Liu, Z.N., Cheng, M.M., Hu, S.M.: Visual attention network. *Computational Visual Media* **9**(4), 733–752 (2023)
17. Hu, J., Shen, L., Sun, G.: Squeeze-and-excitation networks. In: *Proceedings of the IEEE conference on computer vision and pattern recognition*. pp. 7132–7141 (2018)
18. Huang, J.B., Singh, A., Ahuja, N.: Single image super-resolution from transformed self-exemplars. In: *Proceedings of the IEEE conference on computer vision and pattern recognition*. pp. 5197–5206 (2015)
19. Huang, S., Wang, K., Liu, H., Chen, J., Li, Y.: Contrastive semi-supervised learning for underwater image restoration via reliable bank. In: *Proceedings of the IEEE/CVF Conference on Computer Vision and Pattern Recognition*. pp. 18145–18155 (2023)
20. Ji, H., Feng, X., Pei, W., Li, J., Lu, G.: U2-former: A nested u-shaped transformer for image restoration. *arXiv preprint arXiv:2112.02279* (2021)
21. Jiang, Z., Zhang, Y., Zou, D., Ren, J., Lv, J., Liu, Y.: Learning event-based motion deblurring. In: *Proceedings of the IEEE/CVF Conference on Computer Vision and Pattern Recognition*. pp. 3320–3329 (2020)
22. Kong, L., Dong, J., Ge, J., Li, M., Pan, J.: Efficient frequency domain-based transformers for high-quality image deblurring. In: *Proceedings of the IEEE/CVF Conference on Computer Vision and Pattern Recognition*. pp. 5886–5895 (2023)
23. Li, B., Ren, W., Fu, D., Tao, D., Feng, D., Zeng, W., Wang, Z.: Benchmarking single-image dehazing and beyond. *IEEE Transactions on Image Processing* **28**(1), 492–505 (2018)
24. Li, B., Liu, X., Hu, P., Wu, Z., Lv, J., Peng, X.: All-in-one image restoration for unknown corruption. In: *Proceedings of the IEEE/CVF Conference on Computer Vision and Pattern Recognition*. pp. 17452–17462 (2022)
25. Li, F., Shen, L., Mi, Y., Li, Z.: Drcnet: Dynamic image restoration contrastive network. In: *European Conference on Computer Vision*. pp. 514–532. Springer (2022)
26. Li, R., Tan, R.T., Cheong, L.F.: All in one bad weather removal using architectural search. In: *Proceedings of the IEEE/CVF conference on computer vision and pattern recognition*. pp. 3175–3185 (2020)
27. Li, Y., Fan, Y., Xiang, X., Demandolx, D., Ranjan, R., Timofte, R., Van Gool, L.: Efficient and explicit modelling of image hierarchies for image restoration. In: *Proceedings of the IEEE/CVF Conference on Computer Vision and Pattern Recognition*. pp. 18278–18289 (2023)
28. Liang, J., Cao, J., Sun, G., Zhang, K., Van Gool, L., Timofte, R.: Swinir: Image restoration using swin transformer. In: *Proceedings of the IEEE/CVF international conference on computer vision*. pp. 1833–1844 (2021)
29. Liu, H., Dai, Z., So, D., Le, Q.V.: Pay attention to mlps. *Advances in Neural Information Processing Systems* **34**, 9204–9215 (2021)
30. Liu, X., Ma, Y., Shi, Z., Chen, J.: Griddehazenet: Attention-based multi-scale network for image dehazing. In: *Proceedings of the IEEE/CVF international conference on computer vision*. pp. 7314–7323 (2019)

31. Liu, Z., Lin, Y., Cao, Y., Hu, H., Wei, Y., Zhang, Z., Lin, S., Guo, B.: Swin transformer: Hierarchical vision transformer using shifted windows. In: Proceedings of the IEEE/CVF international conference on computer vision. pp. 10012–10022 (2021)
32. Liu, Z., Mao, H., Wu, C.Y., Feichtenhofer, C., Darrell, T., Xie, S.: A convnet for the 2020s. In: Proceedings of the IEEE/CVF conference on computer vision and pattern recognition. pp. 11976–11986 (2022)
33. Luo, X., Xie, Y., Zhang, Y., Qu, Y., Li, C., Fu, Y.: Latticenet: Towards lightweight image super-resolution with lattice block. In: Computer Vision–ECCV 2020: 16th European Conference, Glasgow, UK, August 23–28, 2020, Proceedings, Part XXII 16. pp. 272–289. Springer (2020)
34. Ma, K., Duanmu, Z., Wu, Q., Wang, Z., Yong, H., Li, H., Zhang, L.: Waterloo exploration database: New challenges for image quality assessment models. *IEEE Transactions on Image Processing* **26**(2), 1004–1016 (2016)
35. Martin, D., Fowlkes, C., Tal, D., Malik, J.: A database of human segmented natural images and its application to evaluating segmentation algorithms and measuring ecological statistics. In: Proceedings Eighth IEEE International Conference on Computer Vision. ICCV 2001. vol. 2, pp. 416–423. IEEE (2001)
36. Nah, S., Hyun Kim, T., Mu Lee, K.: Deep multi-scale convolutional neural network for dynamic scene deblurring. In: Proceedings of the IEEE conference on computer vision and pattern recognition. pp. 3883–3891 (2017)
37. Park, D., Kang, D.U., Kim, J., Chun, S.Y.: Multi-temporal recurrent neural networks for progressive non-uniform single image deblurring with incremental temporal training. In: European Conference on Computer Vision. pp. 327–343. Springer (2020)
38. Park, D., Lee, B.H., Chun, S.Y.: All-in-one image restoration for unknown degradations using adaptive discriminative filters for specific degradations. In: 2023 IEEE/CVF Conference on Computer Vision and Pattern Recognition (CVPR). pp. 5815–5824. IEEE (2023)
39. Poirier-Ginter, Y., Lalonde, J.F.: Robust unsupervised stylegan image restoration. In: Proceedings of the IEEE/CVF Conference on Computer Vision and Pattern Recognition. pp. 22292–22301 (2023)
40. Purohit, K., Suin, M., Rajagopalan, A., Boddeti, V.N.: Spatially-adaptive image restoration using distortion-guided networks. In: Proceedings of the IEEE/CVF International Conference on Computer Vision. pp. 2309–2319 (2021)
41. Qin, X., Wang, Z., Bai, Y., Xie, X., Jia, H.: Ffa-net: Feature fusion attention network for single image dehazing. In: Proceedings of the AAAI conference on artificial intelligence. vol. 34, pp. 11908–11915 (2020)
42. Ren, D., Zuo, W., Hu, Q., Zhu, P., Meng, D.: Progressive image deraining networks: A better and simpler baseline. In: Proceedings of the IEEE/CVF conference on computer vision and pattern recognition. pp. 3937–3946 (2019)
43. Shen, Z., Wang, W., Lu, X., Shen, J., Ling, H., Xu, T., Shao, L.: Human-aware motion deblurring. In: Proceedings of the IEEE/CVF International Conference on Computer Vision. pp. 5572–5581 (2019)
44. Song, Y., He, Z., Qian, H., Du, X.: Vision transformers for single image dehazing. *IEEE Transactions on Image Processing* **32**, 1927–1941 (2023)
45. Suin, M., Purohit, K., Rajagopalan, A.: Spatially-attentive patch-hierarchical network for adaptive motion deblurring. In: Proceedings of the IEEE/CVF conference on computer vision and pattern recognition. pp. 3606–3615 (2020)
46. Tian, C., Xu, Y., Zuo, W.: Image denoising using deep cnn with batch renormalization. *Neural Networks* **121**, 461–473 (2020)

47. Tolstikhin, I.O., Houlsby, N., Kolesnikov, A., Beyer, L., Zhai, X., Unterthiner, T., Yung, J., Steiner, A., Keysers, D., Uszkoreit, J., et al.: Mlp-mixer: An all-mlp architecture for vision. *Advances in neural information processing systems* **34**, 24261–24272 (2021)
48. Touvron, H., Bojanowski, P., Caron, M., Cord, M., El-Nouby, A., Grave, E., Izacard, G., Joulin, A., Synnaeve, G., Verbeek, J., et al.: Resmlp: Feedforward networks for image classification with data-efficient training. *IEEE Transactions on Pattern Analysis and Machine Intelligence* **45**(4), 5314–5321 (2022)
49. Touvron, H., Cord, M., Douze, M., Massa, F., Sablayrolles, A., Jégou, H.: Training data-efficient image transformers & distillation through attention. In: *International conference on machine learning*. pp. 10347–10357. PMLR (2021)
50. Trockman, A., Kolter, J.Z.: Patches are all you need? *arXiv preprint arXiv:2201.09792* (2022)
51. Tsai, F.J., Peng, Y.T., Lin, Y.Y., Tsai, C.C., Lin, C.W.: Stripformer: Strip transformer for fast image deblurring. In: *European Conference on Computer Vision*. pp. 146–162. Springer (2022)
52. Tu, Z., Talebi, H., Zhang, H., Yang, F., Milanfar, P., Bovik, A., Li, Y.: Maxim: Multi-axis mlp for image processing. In: *Proceedings of the IEEE/CVF Conference on Computer Vision and Pattern Recognition*. pp. 5769–5780 (2022)
53. Valanarasu, J.M.J., Yasarla, R., Patel, V.M.: Transweather: Transformer-based restoration of images degraded by adverse weather conditions. In: *Proceedings of the IEEE/CVF Conference on Computer Vision and Pattern Recognition*. pp. 2353–2363 (2022)
54. Wang, Z., Cun, X., Bao, J., Zhou, W., Liu, J., Li, H.: Uformer: A general u-shaped transformer for image restoration. In: *Proceedings of the IEEE/CVF conference on computer vision and pattern recognition*. pp. 17683–17693 (2022)
55. Xie, L., Wang, X., Dong, C., Qi, Z., Shan, Y.: Finding discriminative filters for specific degradations in blind super-resolution. *Advances in Neural Information Processing Systems* **34**, 51–61 (2021)
56. Yang, W., Tan, R.T., Feng, J., Liu, J., Guo, Z., Yan, S.: Deep joint rain detection and removal from a single image. In: *Proceedings of the IEEE conference on computer vision and pattern recognition*. pp. 1357–1366 (2017)
57. Yasarla, R., Patel, V.M.: Uncertainty guided multi-scale residual learning-using a cycle spinning cnn for single image de-raining. In: *Proceedings of the IEEE/CVF conference on computer vision and pattern recognition*. pp. 8405–8414 (2019)
58. Zamir, S.W., Arora, A., Khan, S., Hayat, M., Khan, F.S., Yang, M.H.: Restormer: Efficient transformer for high-resolution image restoration. In: *Proceedings of the IEEE/CVF conference on computer vision and pattern recognition*. pp. 5728–5739 (2022)
59. Zamir, S.W., Arora, A., Khan, S., Hayat, M., Khan, F.S., Yang, M.H., Shao, L.: Multi-stage progressive image restoration. In: *Proceedings of the IEEE/CVF conference on computer vision and pattern recognition*. pp. 14821–14831 (2021)
60. Zhang, H., Dai, Y., Li, H., Koniusz, P.: Deep stacked hierarchical multi-patch network for image deblurring. In: *Proceedings of the IEEE/CVF Conference on Computer Vision and Pattern Recognition*. pp. 5978–5986 (2019)
61. Zhang, J., Huang, J., Yao, M., Yang, Z., Yu, H., Zhou, M., Zhao, F.: Ingredient-oriented multi-degradation learning for image restoration. In: *Proceedings of the IEEE/CVF Conference on Computer Vision and Pattern Recognition*. pp. 5825–5835 (2023)

62. Zhang, J., Huang, J., Yao, M., Yang, Z., Yu, H., Zhou, M., Zhao, F.: Ingredient-oriented multi-degradation learning for image restoration. In: Proceedings of the IEEE/CVF Conference on Computer Vision and Pattern Recognition. pp. 5825–5835 (2023)
63. Zhang, K., Li, Y., Liang, J., Cao, J., Zhang, Y., Tang, H., Timofte, R., Van Gool, L.: Practical blind denoising via swin-conv-unet and data synthesis. arXiv preprint arXiv:2203.13278 (2022)
64. Zhang, K., Li, Y., Zuo, W., Zhang, L., Van Gool, L., Timofte, R.: Plug-and-play image restoration with deep denoiser prior. *IEEE Transactions on Pattern Analysis and Machine Intelligence* **44**(10), 6360–6376 (2021)
65. Zhang, K., Luo, W., Zhong, Y., Ma, L., Stenger, B., Liu, W., Li, H.: Deblurring by realistic blurring. In: Proceedings of the IEEE/CVF Conference on Computer Vision and Pattern Recognition. pp. 2737–2746 (2020)
66. Zhang, X., Zeng, H., Zhang, L.: Edge-oriented convolution block for real-time super resolution on mobile devices. In: Proceedings of the 29th ACM International Conference on Multimedia. pp. 4034–4043 (2021)
67. Zhang, Y., Li, D., Shi, X., He, D., Song, K., Wang, X., Qin, H., Li, H.: Kbnnet: Kernel basis network for image restoration. arXiv preprint arXiv:2303.02881 (2023)
68. Zhang, Y., Li, K., Li, K., Wang, L., Zhong, B., Fu, Y.: Image super-resolution using very deep residual channel attention networks. In: Proceedings of the European conference on computer vision (ECCV). pp. 286–301 (2018)
69. Zhao, H., Kong, X., He, J., Qiao, Y., Dong, C.: Efficient image super-resolution using pixel attention. In: Computer Vision–ECCV 2020 Workshops: Glasgow, UK, August 23–28, 2020, Proceedings, Part III 16. pp. 56–72. Springer (2020)
70. Zhou, L., Cai, H., Gu, J., Li, Z., Liu, Y., Chen, X., Qiao, Y., Dong, C.: Efficient image super-resolution using vast-receptive-field attention. In: European Conference on Computer Vision. pp. 256–272. Springer (2022)